Sustainable Cities and Society 100 (2024) 105055

Contents lists available at ScienceDirect

Sustainable Cities and Society

journal homepage: www.elsevier.com/locate/scs

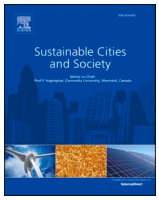

# Evolution of urban morphological polycentricity and the thermal response in Wuhan from 2000 to 2020

Huifang Li [a,b,*], Yujing Han [a], Tao Wang [c], Zhihua Wang [d], Yanan Li [a], Huanfeng Shen [a,b,*]

[a] School of Resource and Environmental Sciences, Wuhan University, Wuhan 430072, China
[b] The Key Laboratory of Geographic Information System, Ministry of Education, Wuhan University, Wuhan 430072, China
[c] China Railway First Survey and Design Institute Group CO., LTD., Xi'an 710043, China
[d] School of Sustainable Engineering and the Built Environment, Arizona State University, Tempe, AZ 85287, USA

ARTICLE INFO

*Keywords:*
Polycentricity/polycentric
Morphological centers
Urban thermal environment
Land surface temperature
High spatio-temporal resolution

ABSTRACT

The emergence of urban polycentric development patterns in response to the pressure of rapid urbanization can profoundly affect the urban heat island (UHI) effect. However, little research has been conducted on this issue at a high spatio-temporal resolution level. To investigate the evolution of urban polycentricity and the accompanying changes in the urban thermal environment, data for 2000 to 2020 from Wuhan in China obtained by multiple sensors were used to extract the urban morphological centers each year and generate annual summer mean land surface temperature (LST) with a 30 m resolution. Results show that the number and size of urban morphological centers in Wuhan increased significantly, from five centers covering 29.75 $km^2$ in 2000 to 15 centers covering 171.72 $km^2$ in 2020. The annual average growth rate was rapid (0.152 $km^2$/a) from 2000 to 2012, then slowed down (0.026 $km^2$/a). The location of newly emerged urban centers aligned with Wuhan's urban development planning. Meanwhile, the urban thermal environment also changed considerably. The summer mean LST have risen by around 1 K, whereas the area of high LST centers fluctuated in the recent two decades. The evolution of urban morphological centers and high LST centers was not always synchronized, with changes in the former showed hysteresis behind the latter, and overlapping areas between the two reaching the maximum at an interval of about nine years. These findings will further our understanding of the urban polycentricity, as well as the evolution of the urban thermal environment in this context.

## 1. Introduction

The world has been experiencing rapid urbanization, and the accompanying urban heat island (UHI) effect is becoming more and more apparent (Chapman et al., 2017; Sussman et al., 2019; Zhang et al., 2020). The UHI effect is manifested as higher temperatures in an urban area than its surrounding rural areas (Oke, 1982), which is affected by multiple natural and human factors, such as climate change, landscape characteristics, urban population density, and residential thermal emission (Ward et al., 2016; Zhou et al., 2019). All these factors are closely related to the advancement of urbanization, during which permeable natural surfaces are constantly being replaced by non-permeable artificial surfaces (Bounoua et al., 2015; Zhang & Huang, 2018), resulting in increased thermal conductivity of the urban ground. It has been confirmed that the increase in UHI intensity has a multifaceted negative impact on human life, including deteriorated resident comfort, a rise in heat-related mortality, and unsustainable development (Akbari & Kolokotsa, 2016; He et al., 2022). Therefore, there is an urgent need to examine the relationship between urban development and the UHI effect in detail.

Previous studies have measured urban development from different perspectives and quantified its contributions to the intensified UHI effect (Hou et al., 2023; Li et al., 2022; Moazzam et al., 2022; Sultana & Satyanarayana, 2020; Yue et al., 2019a). For example, Zhou et al. (2016) explored 32 major cities in China from 2003 to 2012 and found that the UHI effect in almost all of them increased remarkably with the rising urban development intensity (UDI). Similarly, Li et al. (2017) characterized urbanization by urban area expansion and pointed out a significant positive correlation between urban area size and the UHI effect in the conterminous U.S. In addition, some studies have focused on the impact of urban development on the UHI effect for a specific megacity (Kedia et al., 2021; Li et al., 2018; Son et al., 2017). For example, Zhao

* Corresponding authors at: School of Resource and Environmental Sciences, Wuhan University, Wuhan 430072, China.
*E-mail addresses:* huifangli@whu.edu.cn (H. Li), shenhf@whu.edu.cn (H. Shen).

https://doi.org/10.1016/j.scs.2023.105055
Received 25 July 2023; Received in revised form 8 November 2023; Accepted 9 November 2023
Available online 10 November 2023

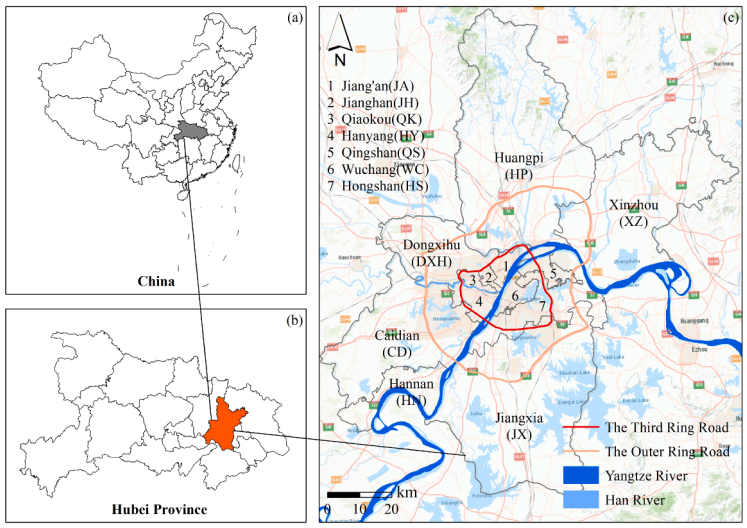


**Fig. 1.** Study area. (a) Location of Hubei Province in China. (b) Location of Wuhan City in Hubei Province. (c) The administrative division of Wuhan and the location of transit circle lines.

et al. (2016) and Xie and Sun (2021) both revealed a high spatial coherence between areas with deteriorating thermal environments and those undergoing rapid urbanization in Shanghai and Wuhan in China. Most of these studies took the city as a whole to analyze the variations of UHI intensity; however, in addition to the outward expansion, the inner structure and development patterns of a city are also constantly changing, leading to more complex changes in the thermal environment within the city.

The transformation of urban development patterns usually implies changes in the landscape configuration within an urban area, which are often measured by alterations of urban land use and land cover (LULC), the density distribution of impervious surfaces, and the relocation of population gathering areas (Alberti, 2005; Artmann et al., 2019; Simwanda & Murayama, 2018; Song, 2005). Therefore, some studies have focused on these characteristics and researched the relationship between urban development patterns and the UHI effect (Qiao et al., 2014; Yang et al., 2010; Yin et al., 2018). For example, Tran et al. (2017) assessed the impact of urbanization-induced LULC changes on the UHI effect and proposed a nonlinear model for predicting LST patterns and UHI intensity. Likewise, Zhou and Chen (2018) studied the change in the UHI intensity of Wuhan between 1965 and 2008 with respect to variations in LULC and urban form (high-density or high-floor) and concluded that there would be a more compact and denser built environment with a serious UHI effect in the future.

However, limited attention has been paid to how the trend of polycentricity affects the thermal environment. As urbanization progresses, the surging population and highly concentrated commercial and industrial activities in the city center highlight the shortcomings of the traditional monocentric structure, causing resource shortages and ecological problems (Finka & Kluvánková, 2015; Hajrasouliha & Hamidi, 2017; Huai et al., 2021). To address this issue, polycentric urban planning has come into view. Polycentricity indicates that a large city contains multiple centers where socioeconomic activities are evenly distributed rather than clustered in one main central area (Anas et al., 1998; Henderson & Mitra, 1996; Homsy & Warner, 2015). The presentation of the urban polycentricity can be shown in the morphology and the function aspects, in which the morphological polycentricity emphasizes on the spatial distribution of the centers, mainly focusing on the relative size of them (Tang & Dou, 2022). This phenomenon of cities expanding in a polycentric pattern on the two-dimensional surface will lead to the changes of LST. From a policy perspective, Kim et al. (2019) explored the link between urban development planning and the transformation of the UHI pattern of Seoul in South Korea and its impact on the temperature of its three urban centers. From the morphological and functional dimensions, Yue et al. (2019b) measured the polycentricity of Hangzhou in China through nighttime light data from 2000 to 2010 and explored its connection with spatio-temporal changes in LST. Specific information on the research concerns, study areas, and quantitative indicators of the relevant literature is shown in Table S1. in supplementary materials.

However, there is still controversy over the approach used to identify urban centers and whether the thermal environment improves due to polycentric development. Moreover, continuous long-term measurement at fine scales remains lacking, due to the data limitations of a single sensor that cannot simultaneously meet the requirements of high spatial and temporal resolutions.

In summary, current researches on urban polycentricity are limited by the data precision, and the relationship between the urban development and the urban thermal environment on a long-time scale remains to be further explored. This paper selected a typical polycentric city, Wuhan, as the study area to analyze its polycentric evolution and summer mean LST changes in the past 20 years. The main contributions of this paper can be summarized as follows:

- An approach to identify the extent of the polycentric centers in a city.
- Generation of annual summer mean LST at 30 m resolution using remote sensing data.
- Analysis of the evolution of the urban morphological centers, the high LST centers and their relations in two decades.

## 2. Materials and methods

### 2.1. Study area

Wuhan is the capital of Hubei province in China and is located at the junction of the Yangtze River and Hanjiang River. It lies between 29° 58′ N to 31° 22′ N latitude and 113° 41′ E to 115° 05′ E longitude, covering an area of 8569.15 km$^2$ (Fig. 1). The city is dominated by flat terrain below 50 m above sea level (Wang et al., 2017), and has a subtropical monsoon climate, with an annual average temperature of 17.3 °C. Based on weather reports collected during 1985 to 2020, the average temperature of Wuhan during summer was 27 °C, the humidity was around 76.05 %, and wind speed was approximately 7 km/h. Wuhan is known as one of the four “oven cities” of China for its hot and long summer, lasting from early May to mid-October each year. Its annual highest temperature usually occurs in July and August (Hubei Meteorological

**Table 1**
The remote sensing data used in this study.

| Sensor/product | Date | Resolution (TIR) |
|---|---|---|
| Landsat 5 TM | 20000913/20031024/20040924/20040722/20060407<br>20070731/20080428/20090906/20110304/20110608 | 30 m |
| Landsat 7 ETM+ | 20010722/20021013/20031101/20040916/20050717<br>20060330/20100917/20110312/20120517/20151017 | 30 m |
| Landsat 8 OLI/TIRS | 20130512/20130613/20141006/20160723/20171030<br>20180408/20180915/20191020/20200803 | 30 m |
| MOD11A1 (daily daytime LST) | 20000914/20010722/20021013/20031101<br>20040916/20050717/20060330/20080506<br>20090906/20100917/20110312/20120517<br>20130614/20141007/20151017/20160724<br>20171031/20180409/20191019/20200804 | 1000 m |
| MOD11A2 (8-day LST) | 20000608/20000624/20000702/20000710/20000726<br>20010609/20010703/20010719/20010812/20010828<br>20020524/20020609/20020703/20020711/20020804/20020820/20020828<br>20030524/20030609/20030617/20030719/20030727/20030804<br>20040608/20040616/20040624/20040702/20040718/20040726/20040803<br>20050617/20050711/20050804<br>20060609/20060617/20060711/20060727/20060812<br>20070601/20070719/20070727/20070804<br>20080531/20080718/20080726/20080803/20080819/20080827<br>20090601/20090609/20090617/20090625/20090711/20090820/20090828<br>20100524/20100601/20100727/20100804<br>20110524/20110601/20110625/20110703/20110719/20110727<br>20120608/20120616/20120726/20120803<br>20130601/20130609/20130711/20130804/20,130820<br>20140524/20140601/20140719/20140728<br>20150727/20150820/20150828<br>20160608/20160616/20160718/20160726/20160811/20160827<br>20170524/20170601/20170711/20170719/20170820<br>20180601/20180609/20180711/20180820/20180829<br>20190601/20190609/20190727/20190804/20190812/20190820/20190828<br>20200811/20200819/20200827 | 1000 m |

Note: The selected MOD11A2 data are denoted by the first day of the 8 days.

Bureau, 2023; Zhang et al., 2023).

On the other hand, Wuhan has experienced rapid urbanization over the past 20 years. In this process, the trend of polycentric in Wuhan's urban planning has become more obvious. "Wuhan City Master Plan (1996–2020)" proposed the "polycentric group" layout concept, which divided the city into three circles. It emphasized the formation of two core areas on two sides of the Yangtze River, 10 central districts around the core areas, and 10 integrated clusters on the periphery. Two subsequent revisions and improvements, in 2010 and 2017, further specified the location and function of the urban centers. These features make Wuhan a quite suitable case for studying polycentric development and summer LST distribution.

### 2.2. Data

The data captured by the Landsat 5 Thematic Mapper (TM), Landsat 7 Enhanced Thematic Mapper Plus (ETM+), and Landsat 8 Operational Land Imager/Thermal Infrared Sensor (OLI/TIRS), and the Terra MODIS LST products (MOD11A1 and MOD11A2) for each summer from 2000 to 2020 (Table 1) were used in this study. All the data was retrieved from the official website of the United States Geological Survey (USGS) (https://earthexplorer.usgs.gov/). The visible bands of the Landsat data were used to identify the urban morphological centers, and the thermal infrared bands (TIR) were used to retrieve the fine-resolution (30 m) LST, as a reference for the data fusion. Considering the long summer of Wuhan, high-quality images ranging from May to October with a cloud amount of less than 5 % were selected.

The MODIS products included the daily daytime LST product MOD11A1 and the 8-day LST product MOD11A2, spanning the same period as the Landsat data. The MOD11A1 data were used as the reference data with a coarse resolution (1 km) for the spatio-temporal fusion, and the MOD11A2 data were used to calculate the annual summer mean LST.

In addition, all the satellite data were rectified to the Universal Transverse Mercator (UTM) projection system (spheroid WGS84, datum WGS84, and zone 49). Furthermore, due to the failure of the scan line corrector (SLC) on Landsat 7 in 2003, the multi-temporal regression and regularization method (Li & Becker, 1993) was used to recover the missing information.

### 2.3. Identification of urban morphological centers

A high coverage of artificial impervious surfaces is the most representative feature of urban areas. Urban impervious surface refers to the artificial surface cover on which water cannot infiltrate directly into the soil, including types of buildings, roads, squares, etc. On the one hand, it indicates intense human activity zones, which are more developed than the surroundings. On the other hand, the area of impervious surface has been shown to have a positive correlation with LST, due to its hydrothermal properties (Yang et al., 2016). Therefore, in this study, the aggregation degree of impervious surfaces was utilized to identify urban morphological centers and further explore the relationship with LST.

#### 2.3.1. Extraction of urban impervious surfaces

Medium-resolution remote sensing images usually have a spatial resolution of tens of meters and therefore commonly contain mixed pixels, within which multiple ground objects exist. For this feature, pixel unmixing is often used to decompose the proportion of the endmembers in each pixel. Based on this method, the vegetation-impervious surface-soil (V-I-S) model (RIDD, 1995) was proposed. This model regards the urban surface as a linear combination of three pure endmembers: vegetation, impervious surface, and soil. In this study, we utilized linear spectral mixture analysis (LSMA) combined with the V-I-S model to obtain the impervious surface abundance (i.e., the percentage of impervious surface in each pixel), to further identify the urban morphological centers.

Considering that primary materials used for the buildings and roads may have changed over years, and their different physical properties can be reflected in reflectance spectral characteristics, so we selected a variety of end member types of impervious surfaces based on the remote sensed reflections for each year. Accordingly, the primary impervious surface endmember used in the V-I-S model was divided into finer categories, i.e., cement, fiber cement, color steel tile, asphalt, red brick, and other categories, according to their materials. Vegetation and soil, together with these finer categories, were taken as the pure endmembers for LSMA. High-quality Landsat images covering the urban area of Wuhan from 2000 to 2020 were processed, and pixels with an impervious surface abundance over 0.5 (added up the percentage of different building materials) were finally extracted as the urban impervious surface for further urban center identification.

#### 2.3.2. Boundary effect considered kernel density estimation (BEKDE)

When analyzing the spatial distribution of discrete sample points, i.

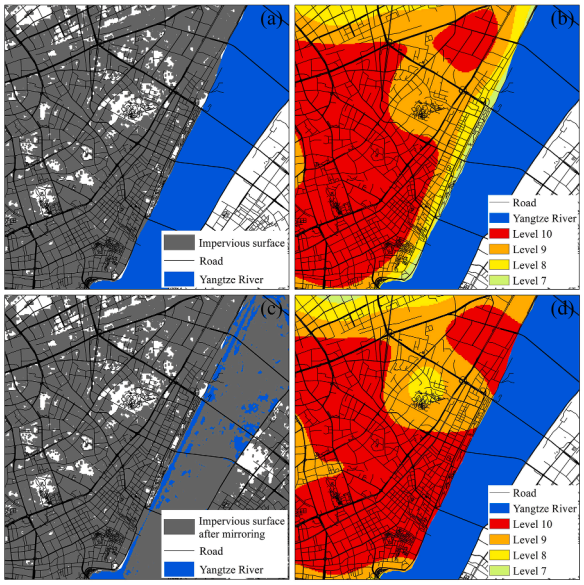


**Fig. 2.** Schematic diagram of the boundary effect considered kernel density estimation (BEKDE) method. (a) Impervious surface distribution on the left river bank of the Yangtze River. (b) Initial KDE (before improvement) result. (c) Distribution of impermeable surfaces after symmetrically extending the data points according to the spatial boundaries. (d) Boundary effect considered KDE (after improvement) result.

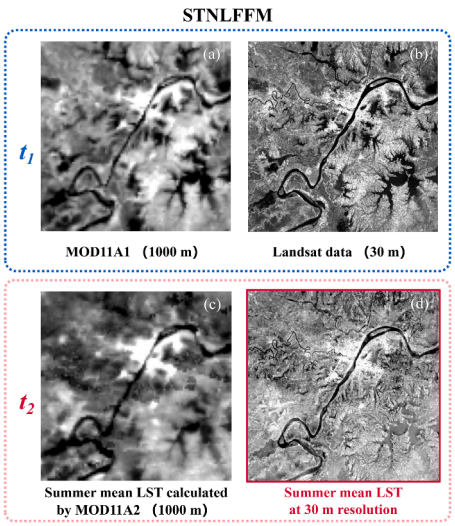


**Fig. 3.** Spatio-temporal fusion framework for the generation of summer mean LST at 30 m resolution. (a) MOD11A1(daily product) as the "coarse-resolution" image at the reference date. (b) Retrieved LST from Landsat data as the "fine-resolution" image at the same/close moment as (a). (c) The summer mean LST calculated by MOD11A2 (8-day product) as the "coarse-resolution" image at the target date. (d) Fused summer mean LST at 30 m resolution.

e., impervious surface pixels in this study, it is often desirable to obtain their continuous density distribution. The kernel density estimation (KDE) method is a classical non-parametric method for estimating a probability density function that calculates the unit density of the value of a point element over a specified range of neighborhoods, thus visualizing the distribution of discrete data points over a continuous area. However, in practical scenarios, the distribution of sample points is often influenced by topographical features. For example, since ancient times, human beings have always tended to settle along rivers due to the fertile soil on the river banks and expand their settlements to both sides as the population grows. This phenomenon can lead to serious misestimation at river boundaries when performing KDE, as it assumes a smooth distribution when estimating the local density. To address this boundary effect problem, relevant studies have been conducted to improve the KDE method. In a one-dimensional (1D) scenario, by mirroring the sample points to the other side of the boundary, a symmetrically distributed sample is obtained, and then KDE is performed to obtain a reasonable sample density at the boundary (Jones, 1993). In a two-dimensional (2D) scenario, this issue has not received sufficient attention. Only a few scholars have used the approach of symmetrically extending the data points to the other side of the boundary to obtain accurate density distribution estimates (e.g., Benhamou& Cornélis, 2010). Consequently, inspired by the idea of mirroring data, we propose the boundary effect considered kernel density estimation (BEKDE) method for application with remote sensing data. In the following, we specifically explain the boundary effect problem and the proposed BEKDE method, in combination with Fig. 2.

As shown in Fig. 2(a), the Yangtze River runs through the center of Wuhan, dividing the city into two parts, and the impervious surface area is distributed densely at the river frontage (taking the left bank as an example). The KDE results significantly underestimate the impervious surface density at such boundaries, as shown in Fig. 2(b), where the patches from red to blue mean decreasing density in descending order, and a clear gradient of decreasing density can be seen in the area near the river. When applying the proposed BEKDE method, a straight line approximating the boundary of the river was taken as the axis of symmetry, and then the impervious surface data points were mirrored, as shown in Fig. 2(c). Finally, KDE was performed to obtain the heat map of each side without boundary effects, as shown in Fig. 2(d), with the help of ArcGIS 10.6 software. After several trials, we set the bandwidth as 1800 m, ensuring a moderately smooth visual effect.

To obtain the urban morphological centers, the results of the BEKDE method were divided into 10 levels according to the natural breaks (Jerks) method (Mills, 2008), and the patches at level 10 were identified as the urban morphological centers.

### 2.4. Identification of high LST centers

#### 2.4.1. Generation of annual summer mean LST

The thermal bands of the Landsat data in each summer from 2000 to 2020 were used to retrieve the LST using a single-channel temperature retrieval method (Jiménez-Muñoz & Sobrino, 2003; Sobrino & Raissouni, 2000). STNLFFM (Cheng et al., 2017) was used to generate the summer mean LST with a high spatial resolution. In STNLFFM, a pair of images at the reference date ($t_1$), one with a low spatial resolution but a high temporal frequency ("coarse-resolution" image) and the other with a high spatial resolution but a low temporal frequency ("fine-resolution" image), and also a coarse-resolution image at the target date ($t_2$), are required to generate the fine image at the target date through data fusion. In this study, the LST retrieved by the Landsat data (30 m) was taken as the fine-resolution images and the MOD11A1 data as the coarse-resolution images at $t_1$, together with the summer mean LST calculated with several available MOD11A2 images in each year as a reference image at $t_2$.

The details of the data fusion method are provided in Fig. 3.

#### 2.4.2. High LST center identification based on BEKDE

Firstly, the summer mean LST was divided into five levels (*low, sub-low, medium, sub-high*, and *high*), according to the standard deviation method, as shown in Table 2. The BEKDE method introduced in *Section 2.3.2.* was then performed on the *high* level LST to identify the high LST centers.

### 2.5. Overall framework

The overall flowchart of this research is shown in Fig. 4.

**Table 2**
Levels of LST.

| LST Level | *Low* | *Sub-low* | *Medium* | *Sub-high* | *High* |
|---|---|---|---|---|---|
| Range | $TS \leq \mu - 1.5std$ | $\mu - 1.5std < TS \leq \mu - 0.5std$ | $\mu - 0.5std < TS \leq \mu + 0.5std$ | $\mu + 0.5std < TS \leq \mu + 1.5std$ | $TS > \mu + 1.5std$ |

Note: $T_s$ is the summer mean LST value of a specific raster, $\mu$ is the mean value of summer mean LST and *std* is the standard deviation of summer mean LST.

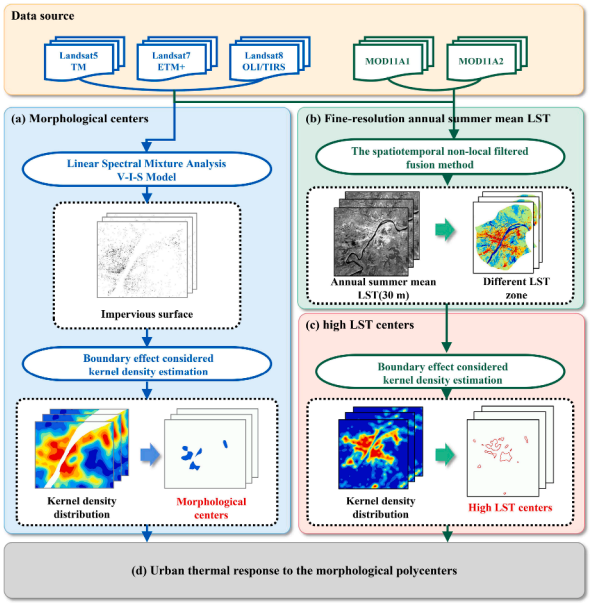


**Fig. 4.** Overall flowchart consisting of four key steps. (a) Identification of urban morphological centers. (b) Generation of annual summer mean LST at a fine-resolution level. (c) Identification of high LST centers. (d) Analyzation of the relationship between the urban morphological centers and the high LST centers.

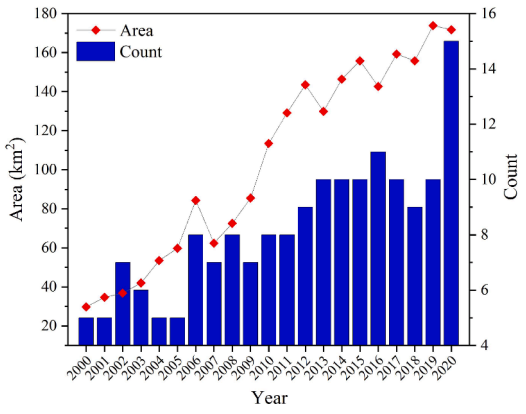


**Fig. 5.** The number and area variation of the urban morphological centers in Wuhan.

## 3. Results

### 3.1. Urban morphological centers from 2000 to 2020

Wuhan's polycentric development has been pronounced over the past two decades. The built-up area has gradually expanded beyond the Third Ring Road. The old urban area has not changed much due to the constraint of space, with building heights ranging from 20 to 40 m. However, the area outside the Third Ring Road has changed dramatically, building up from nothing, with building heights ranging from 6 to 25 m. The number and size of the urban morphological centers in Wuhan have shown an increasing trend from 2000 to 2020. Fig. 5 shows the change in the number and total area of the urban morphological centers in Wuhan from 2000 to 2020. The total area of the urban centers increased rapidly from 2000 to 2012, with an annual average growth rate of 0.152 $km^2$/a, and then fluctuated slowly from 2013 to 2020, with an annual average growth rate of 0.026 $km^2$/a.

Considering both the number and the distribution (Fig. 6) of the urban centers, the polycentric development in Wuhan can be divided into three phases, except for 2020, taking 2005 and 2011 as the breakpoints. From 2000 to 2005, the number of urban centers was maintained at around five, with all the urban centers distributed in the main urban area (within the Third Ring Road), except for Qingshan (QS). In addition, it should be noted that, since 2002, two new urban centers—Qiaokou (QK) and Jiang'an (JA)—have emerged, and there has been a clear tendency for the inherent urban center (Jianghan (JH)) to merge with these new urban centers. In this phase, the new urban centers were still attached to the inherent urban centers and tended to emerge around them. From 2006 to 2011, the number of urban centers was stable at seven to eight. However, the old and new centers alternated dramatically during this phase, as reflected in the germination of the Dongxihu (DXH) center and the convergence of the Qiaokou1 (QK1) and Qiaokou2 (QK2) centers. In addition, a new center (Wuchang-Hongshan-Qingshan2 (WHQ2)) appeared at the junction of the Wuchang and Honghsan districts and converged with WHQ1 to form a larger center. From 2012 to 2019, the largest center (Jiang'an-Jianghan-Qiaokou (JJQ)) spanning the three districts inside the main urban area began to take shape, and at the same time, small new urban centers (Hanyang2 (HY2), Jiangxia1(JX1), Hongshan1 (HS1) and Caidian1 (CD1)) appeared far away from the main urban area, mostly located in the west and southeast. Finally, we take 2020 as a separate phase, when some small patch centers (Hongshan2 (HS2), Hongshan3 (HS3), Jingxia2 (JX2), Caidian2 (CD2), and Caidian3 (CD3)) suddenly appeared in the suburbs. In general, the development of polycentricity in Wuhan has been obvious over the past 21 years, with the number and area of urban centers growing from five and 29.75 $km^2$ in 2000 to 12 and 171.72 $km^2$ in 2020. The development rate was first rapid and then slow, and the whole process was accompanied by the emergence of new centers and the merging of old and new centers.

### 3.2. Urban high LST centers in summer from 2000 to 2020

#### 3.2.1. Accuracy of summer mean LST

The accuracy of the obtained fine-resolution summer mean LST data was quantitatively assessed. The summer mean LST for each year directly calculated from the MOD11A2 data was taken as the actual value, and that of our fusion result was taken as the measured value. We used both absolute and relative error metrics. The former, i.e., the mean absolute error (MAE), is the average of the absolute value of the difference between the two, and the latter, i.e., the mean relative error (MRE), is the ratio of the mean absolute value of the difference to the actual value. The data were kept at the same spatial resolution before calculation. The results show that the relative errors from 2000 to 2020 are generally less than 0.56 %, and the absolute errors are less than 1.7 K (Fig. 7). Therefore, we can conclude that the fusion accuracy is precise enough for the follow-up analysis.

#### 3.2.2. Summer mean LST from 2000 to 2020

Fig. 8 and Fig. 9 show the variation of the annual summer mean LST and the area proportion of each LST zone during the study period,

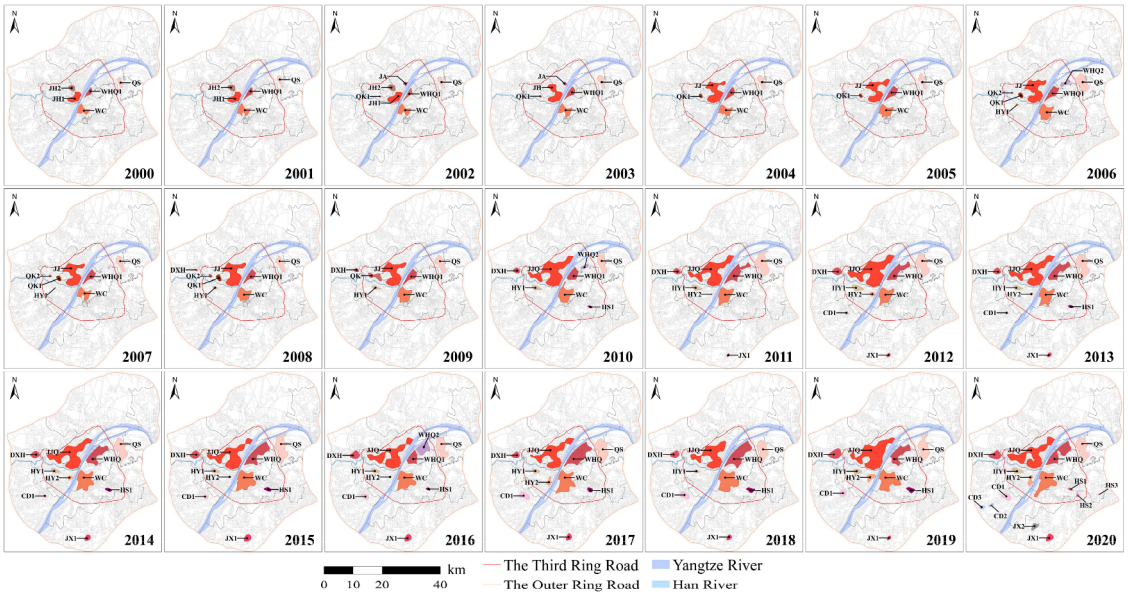


**Fig. 6.** Urban morphological centers in Wuhan from 2000 to 2020.
Note: The urban morphological centers are marked with the abbreviation of the name of the district in which they are located: JH (Jianghan), JA (Jiang'an), QK (Qiaokou), JJ (Jiang'an-Jianghan), JJQ (Jiang'an-Jianghan-Qiaokou), HY (Hanyang), WC (Wuchang), HS (Hongshan), QS (Qingshan), WHQ (Wuchang-Honghan-Qingshan), DXH (Dongxihu), CD (Caidian), JX (Jiangxia). When more than one center appears in the same district, followed by an Arabic numeral to differentiate.

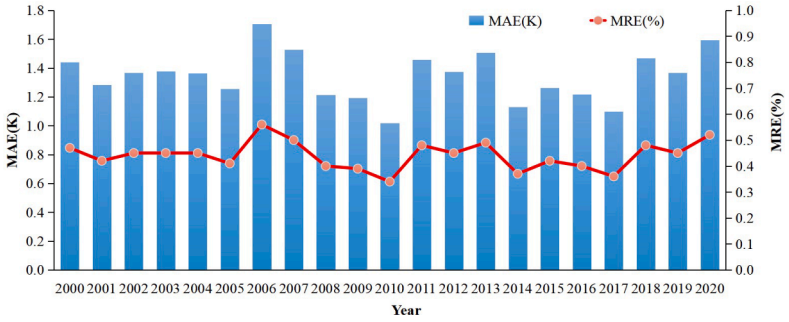


**Fig. 7.** Fusion accuracy measured by mean absolute error (MAE) and mean relative error (MRE).

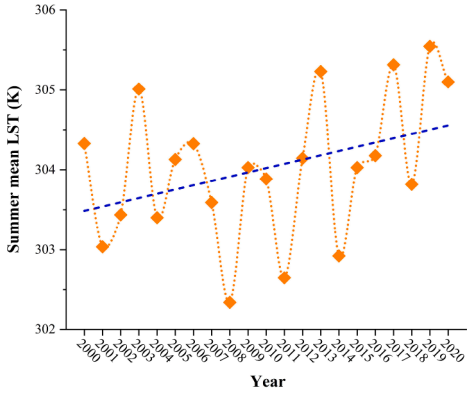


**Fig. 8.** Variation of the summer mean LST in Wuhan from 2000 to 2020.

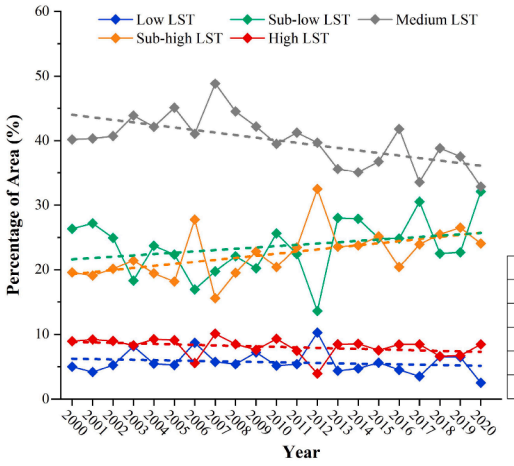


| Series | slope |
|---|---|
| Low LST | -0.06 |
| Sub-low LST | 0.2 |
| Medium LST | -0.39 |
| Sub-high LST | 0.32 |
| High LST | -0.08 |

**Fig. 9.** Area percentage of different LST zones per year in Wuhan.

respectively. The average of the summer mean LST in the study area from 2000 to 2020 was around 304.02 K (±1.5 K), the maximum value (305.54 K) occurred in 2019 and the minimum value (302.34 K) occurred in 2008. The summer mean LST shows a fluctuating upward trend, increasing by about 1 K from 2000 to 2020. More specific evolution trends need to be illustrated in conjunction with the results of the classification results. As shown in Fig. 9, the *medium* LST zone has the largest area proportion, reaching about 40 % of the total area, with LST values around 305 K. The *sub-low* and *sub-high* LST zones have the second largest area proportion, with LST around 303 K and 307 K,

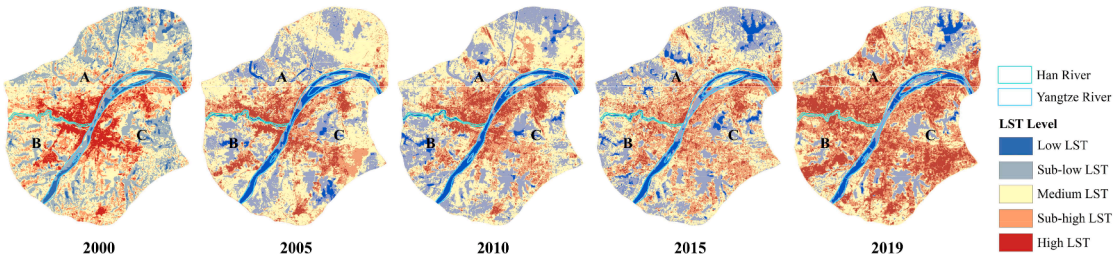


**Fig. 10.** Urban summer mean LST of Wuhan in 2000, 2005, 2010, 2015 and 2019.
Note: A, B, C represents the three regions separated by the Yangtze and Han Rivers, respectively. The summer mean LST in 2019 rather than 2020 is shown to avoid the influence of the special event (COVID-19) in 2020.

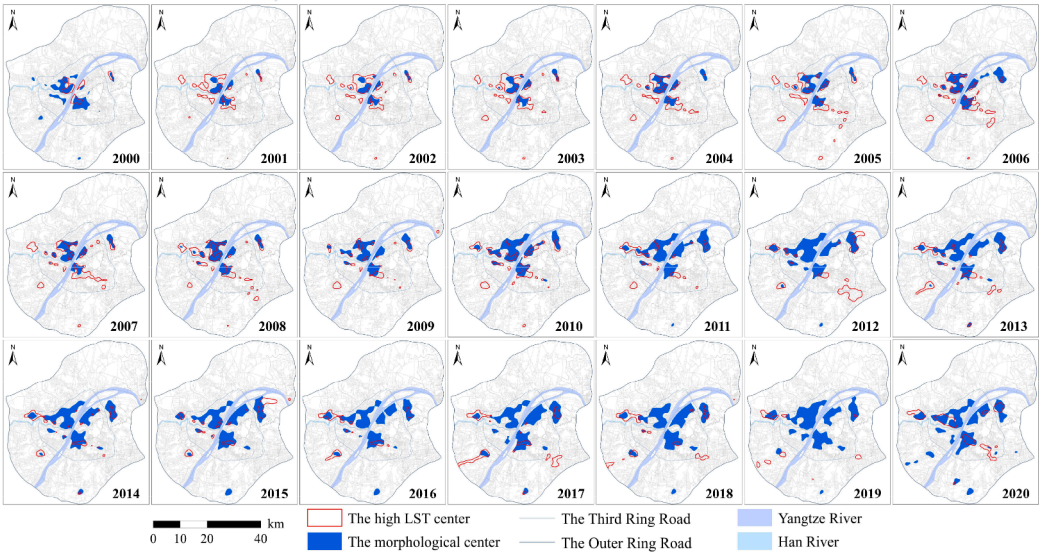


**Fig. 11.** Identified high LST centers in Wuhan from 2000 to 2020.

respectively, and the *low* and *high* LST zones have the smallest area proportion, with LST below 308 K and above 300 K, respectively. The *sub-high* LST zone has shown an obvious expanding trend, with an increase of about 5 % in its proportion, while the *medium* LST zone has shown a clear reducing trend, with a slop of −0.39. As for the *high* and *low* LST zones, there were no significant changes in the area proportion. This warming phenomenon synchronized with the expansion of impervious surfaces and can significantly affect thermal comfort (Li et al., 2021).

To obtain a more detailed understanding of the changes in LST distribution, we explored its spatial characteristics every five years (Fig. 10). The study area is divided into three sectors (A, B and C) by the Yangtze and Han rivers. In region A, there has been a clear expansion of the *high* LST zone, mainly westwards along the Han River, and there are also emerging *high* LST patches near the other small tributaries of the Yangtze River in the north. In region B, the *high* LST and *sub-high* LST zones have expanded in an overall south-westerly direction. In region C, the *high* LST zones located in the north, central and south have all shown an expanding trend. At the same time, the area of the *sub-high* LST zone has increased throughout the region. However, it should be noted that, although there has been a significant expansion of *high* LST zones outside the main urban area, the density of the original *high* LST patches in the main urban area has decreased, which is why there has been no significant increase in the percentage of *high* LST zone. Similarly, the study of Deng et al. (2023) also found that as Wuhan developed, building densification at the edge of the main urban area led to warming and thus reduced thermal comfort, while the correlation between building density and temperature within the main urban area was not high.

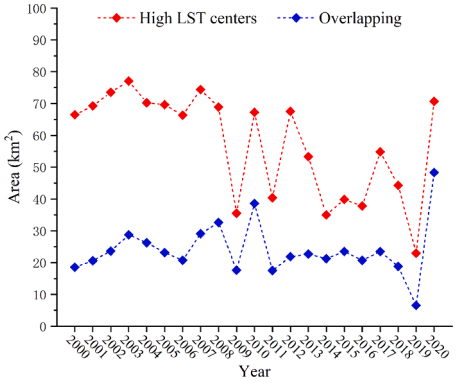


**Fig. 12.** The area of the high LST centers and the overlapping area of the morphological centers and the high LST centers in Wuhan from 2000 to 2020.

### 3.2.3. *High LST centers and their characteristics*

Similar to the urban morphological centers, the high LST centers also displayed a distinct polycentric distribution. With the migration of the population and economic activities from the main urban area, there has been a trend of suburbs and even small towns or villages developing into new urban centers. The growth of the polycentricity mentioned above has resulted in the rapid expansion of impervious surfaces from the initial urban centers assembled within the main urban area to new urban centers distributed outside the main urban area. At the same time, this process has also been accompanied by temperature fluctuation. To

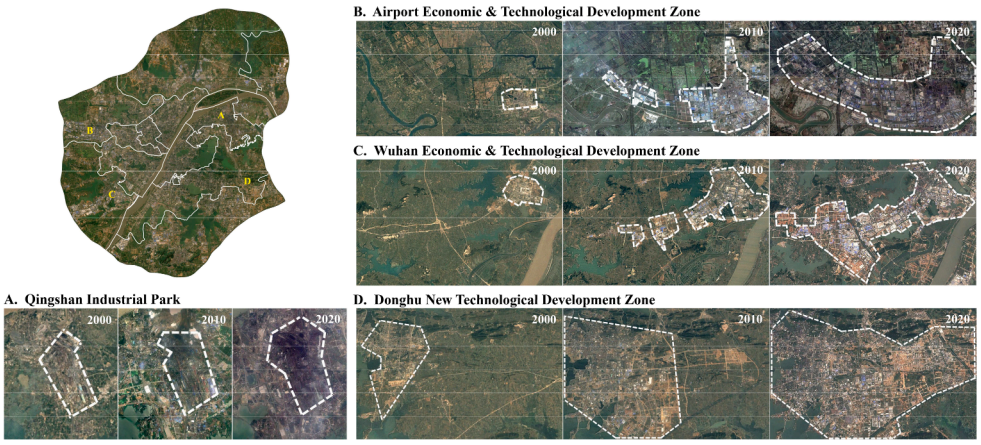


**Fig. 13.** The development of the Qingshan industrial zone and three Economic & Technological Development Zones in Wuhan.

establish the influence of polycentricity on LST, we analyzed the spatial association of the urban morphological centers and the high LST centers. Figs. 11 and 12 show the spatial distribution of the high LST centers and the variation of the total overlapping area of the two types of centers, respectively. The distribution of high LST centers was quite different from that of morphological centers, with a more fragmented morphology and more dramatic inter-annual variability. From 2000 to 2010, high LST centers were concentrated in the main urban area. From 2011 onwards, they had a clear tendency to migrate out of the Third Ring Road, the area of them within the main urban area was greatly reduced, and the area of morphological centers overlapping with them was maintained at a low level. By around 2018, high LST centers were distributed only outside the Third Ring Road, and the overlapping area was confined to the west where the DXH (Dongxihu) center was located, while by 2020 the high LST centers reappeared in a large area inside the Third Ring Road, and the overlapping area of the two types of centers reached the maximum value of 69.8 $km^2$. Meanwhile, the overlapping area between high LST centers and morphological centers has fluctuated considerably since 2010, and the changing trend was almost the same as that of high LST centers.

## 4. Discussion

### 4.1. Polycentric evolution of urban morphological centers

Over the past two decades, Wuhan's urbanization rate continued to grow, accompanied by an increase in its residential population. Although such development can effectively promote economy, it has also brought a range of ecological problems (Theodorou, 2022; Yao et al., 2021), such as green space loss (Puplampu & Boafo, 2021), increased pollution (Liang et al., 2019), and local climate deterioration (Qian et al., 2022). To achieve sustainable development and rationalize the allocation of urban resources, Wuhan's urban planning from 2000 to 2020 has gradually clarified the concept of polycentricity. It should also be noted that differing from conventional sub-centers, these planned urban centers are larger and more functional, with mature housing, entertainment, services, and infrastructure (Cheng & Masser, 2003).

According to the urban morphological center extraction results (Fig. 6), the inherent centers in 2000 were all located in the main urban area, except for the QS center in the northeast. This is mainly because the main urban area was dominated by residential, commercial and educational land uses with a dense distribution of impervious surfaces, while QS District as an old chemical zone, was built before 2000 and was similarly distributed with large areas of impervious surfaces. Subsequently the centers within the main urban area expanded in size and gradually connected, however the shape of the expansion and the location where the linkage occurred were random without a clear pattern. This is possibly a result of some fragmented green space configurations. As time elapsed, new urban morphological centers gradually emerged outside the Third Ring Road, and these new centers appeared successively in Dongxihu District in the west, Caidian District in the southwest, and Hongshan District in the east. These areas are important economic development zones or industrial areas that have seen rapid development in recent years and a significant increase in impervious surface density. Around 2010, in addition to the main urban area, which remained as the central activity zone, these three new core areas gradually taking shape and sharing some of the urban functions, and their locations correspond to the three aforementioned District (Fig. 13.(a)). At present, in the "Wuhan City Master Plan (2017–2035)", the city presents the pattern of "one main center plus three sub-centers plus three new clusters", making the goal of polycentric development clearer. One main center means the main urban area, and the three sub-centers take the three economic and technological development zones (B, C and D in Fig. 13(a)) as the cores, and the three new clusters refer to the eastern, southern, and western town clusters radiating outward from the three sub-centers. The leading role of policies in Wuhan's polycentricity development process is obvious.

### 4.2. Polycentric evolution of urban high LST centers and its relation to urban morphological centers

The high LST centers varied more dramatically between years than morphological centers because of the more complex causes affecting LST, however, an overall fluctuating down ward trend can still be observed. The high LST centers were gradually shifting outward from the main urban area, and the locations of these new centers appearing and expanding also correspond to the four economic and industrial zones in Fig. 13. This is because outside of the main urban areas, impervious surfaces largely replaced the natural surface, and these areas are mainly industrial sites and economic and technological development zones, which can produce more heat than human life in the main urban areas.

Based on the results of the superposition analysis of the urban morphological centers and high LST centers, it can be found that the high LST centers do not always coincide with the geographical distribution of the urban morphological centers as much as expected. Especially after 2010, the high LST centers did not appear in the central area but moved to the suburbs away from the central area. An interesting phenomenon related to this is that the urban morphological centers always appeared later than the high LST centers. Taking the situation in 2000 as an example, high LST centers were distributed in the region south of the Han River, and to the west, south, and east of the Third Ring Road, where urban morphological centers had not yet formed. Specifically, the high LST centers located in Hanyang District did not include

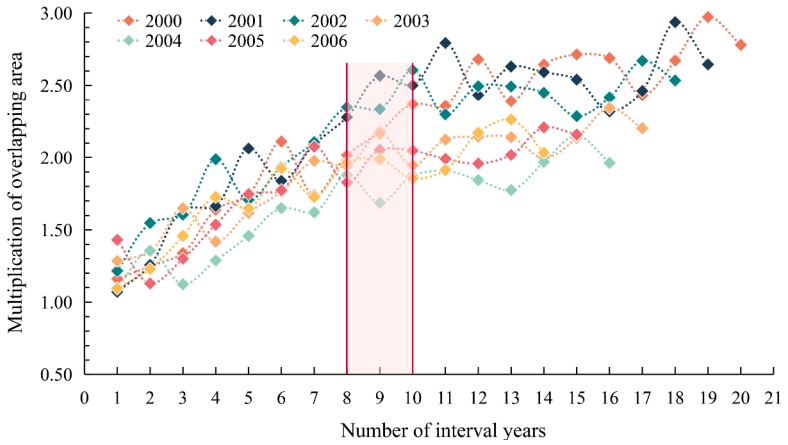


**Fig. 14.** Multiplicative increase in the area of overlap between urban morphological centers and high LST centers for different interval years.

urban morphological centers until 2006. This phenomenon continued throughout the study period. Therefore, we further superimposed the high LST centers of the earlier years with the urban morphological centers of the later years and set incremental interval years. Fig. 14 illustrates the ratio of the overlapping area after temporal misalignment to that in the current year. It shows that the hysteresis phenomenon of the urban morphological centers is quite obvious. The area of overlap after temporal misalignment first increased and then fluctuated with the increase of the interval years. At the same time, we conducted the Mann-Kendall test (Kendall, 1973; Mann, 1945), a common nonparametric method for trend determinations on time-series data, and the results demonstrate that the overlapping area reaches its maximum at an interval of about nine years. Combined with the geographical location, most of the areas where the high LST centers predicted the emergence of urban morphological centers mostly consisted of residential and industrial land. Due to strong domestic heat production and active industrial production activities, high LST centers are detected earlier, while impervious surfaces increase relatively slowly, resulting in a hysteresis in the formation of the urban morphological centers. Based on this fact, urban planners could adjust their strategies according to the distribution of high LST centers.

### 4.3. Analysis of the specificity of 2020 in Wuhan

About the unusually large area of overlap seen between urban morphological centers and high LST centers in 2020, possible causes were investigated. Since it is almost impossible for natural factors to change drastically in a short period, the main reason considered is the outbreak of COVID-19. Firstly, the intensity of urban production outside the main urban area was lower than before, the impervious surface changes were minimal, and human activity areas were clustered in residential and commercial areas within the third ring road. Secondly, the development of new centers was mainly dependent on migrant and local populations, while the lockdown of communities and streets severely limited the number of migrants. Besides, the statistical yearbook shows that the proportion of the resident population in the main urban area of Wuhan was over 60 % at the end of 2019, which means that the economic activities became more concentrated in the central city where the resident population lives on a routine basis.

The above discussion on the results for 2020 is speculative based on the existing data and the actual situation. To establish the real reasons for the "outliers" in 2020, on the one hand, the effect of spatial information alternations in the data fusion needs to be further excluded. On the other hand, if we consider 2020 as not a sudden situation, but as the starting point of a new transformation of urban form and LST distribution patterns, then it will be necessary to take a longer-term view and explore a wider time series in future studies.

## 5. Conclusions and future work

This paper reveals the spatial and temporal distribution patterns and evolutionary characteristics of urban morphological centers and high LST centers of Wuhan from 2000 to 2020 at 30 m resolution.

For the urban morphological centers, the number and area growth of them is first fast (0.152 $km^2$/a) and then slow (0.026 $km^2$/a), and the location of the new centers expands outward from the main urban area, which is highly consistent with the city master plan. For the thermal environment and high LST centers, the summer mean LST have risen by about 1 K, with the proportion of *sub-high* LST zone increased by about 5 %, which may be related to the new morphological centers are mainly found in industrial zones and economic and technological development zones where heat production is high. Whereas the area of high LST centers fluctuated in the recent two decades. As for the association between the two types of centers, they do not always locate in the same area, the urban morphological centers show an obvious hysteresis effect, appearing after the high LST centers by about nine years, so this "predictable" phenomenon can provide some reference for urban planning. Moreover, the recovery of the high LST centers with in the Third Ring Road in 2020 can be mainly attributed to the intensified life within the main urban area because of the city lockdown during the COVID-19 pandemic.

For future work, there are still some outstanding issues worth further investigation in this field. The continuous and long time-series categorized data on urban functional areas, which if available would help to reveal more about the relationship between urban polycentricity and thermal environment. Moreover, a longer time scale study is still necessary to clarify whether 2020 is an exceptional case or the beginning of a new evolutionary phase.

## Declaration of Competing Interest

We declare that we have no financial personal relationships with other people or organizations that can inappropriately influence our work, and there is no professional or other personal interest of any nature or kind in any product, service, and/or company that could be construed as influencing the position presented in, or the review of, the manuscript entitled.

## Data availability

The data that has been used is confidential.

## Acknowledgment

This work was funded by the National Key Research and Development Program of China (2022YFF1301103). Key Research and Development Program of Hubei Province Grant/Contract number: 2023BAB066.

## Supplementary materials

Supplementary material associated with this article can be found, in the online version, at doi:10.1016/j.scs.2023.105055.

## References

Akbari, H., & Kolokotsa, D. (2016). Three decades of urban heat islands and mitigation technologies research. *Energy and Buildings, 133*, 834–842. https://doi.org/10.1016/j.enbuild.2016.09.067

Alberti, M. (2005). The effects of urban patterns on ecosystem function. *International Regional Science Review, 28*(2), 168–192. https://doi.org/10.1177/0160017605275160

Anas, A., Arnott, R., & Small, K. (1998). Urban spatial structure. *Journal of Economic Literature, 36*, 1426–1464.

Artmann, M., Inostroza, L., & Fan, P. (2019). Urban sprawl, compact urban development and green cities. How much do we know, how much do we agree? *Ecological Indicators, 96*, 3–9. https://doi.org/10.1016/j.ecolind.2018.10.059

Benhanmou, S., & Cornélis, D. (2010). Incorporating movement behavior and barriers to improve kernel home range space use estimates. *The Journal of Wildlife Management, 74*(6), 1353–1360. https://doi.org/10.1111/j.1937-2817.2010.tb01257.x

Bounoua, L., Zhang, P., Mostovoy, G., Thome, K., Masek, J., Imhoff, M., & Toure, A. M. (2015). Impact of urbanization on US surface climate. *Environmental Research Letters, 10*(8). https://doi.org/10.1088/1748-9326/10/8/084010

Chapman, S., Watson, J. E. M., Salazar, A., Thatcher, M., & McAlpine, C. A. (2017). The impact of urbanization and climate change on urban temperatures: A systematic review. In *Landscape ecology, 32* pp. 1921–1935). Netherlands: Springer. https://doi.org/10.1007/s10980-017-0561-4. Issue.

Cheng, J., & Masser, I. (2003). Urban growth pattern modeling: A case study of Wuhan city, PR China. *Landscape and Urban Planning, 62*(4), 199–217. https://doi.org/10.1016/S0169-2046(02)00150-0

Cheng, Q., Liu, H., Shen, H., Wu, P., & Zhang, L. (2017). A spatial and temporal nonlocal filter-based data fusion method. *IEEE Transactions on Geoscience and Remote Sensing, 55*(8), 4476–4488. https://doi.org/10.1109/TGRS.2017.2692802

Deng, X., Cao, Q., Wang, L., Wang, W., Wang, S., Wang, S., & Wang, L. (2023). Characterizing urban densification and quantifying its effects on urban thermal environments and human thermal comfort. *Landscape and Urban Planning, 237*, Article 104803. https://doi.org/10.1016/j.landurbplan.2023.104803

Finka, M., & Kluvánková, T. (2015). Managing complexity of urban systems: A polycentric approach. *Land Use Policy, 42*, 602–608. https://doi.org/10.1016/j.landusepol.2014.09.016

Hajrasouliha, A. H., & Hamidi, S. (2017). The typology of the American metropolis: Monocentricity, polycentricity, or generalized dispersion? *Urban Geography, 38*(3), 420–444. https://doi.org/10.1080/02723638.2016.1165386

He, B. J., Wang, J., Zhu, J., & Qi, J. (2022). Beating the urban heat: Situation, background, impacts and the way forward in China. In *Renewable and sustainable energy reviews, 161*. Elsevier Ltd. https://doi.org/10.1016/j.rser.2022.112350

Henderson, V., & Mitra, A. (1996). The new urban landscape: Developers and edge cities. *Regional Science and Urban Economics, 26*(6), 613–643. https://doi.org/10.1016/S0166-0462(96)02136-9

Homsy, G. C., & Warner, M. E. (2015). Cities and sustainability. *Urban Affairs Review, 51*(1), 46–73. https://doi.org/10.1177/1078087414530545

Hou, H., Longyang, Q., Su, H., Zeng, R., Xu, T., & Wang, Z. H. (2023). Prioritizing environmental determinants of urban heat islands: A machine learning study for major cities in China. *International Journal of Applied Earth Observation and Geoinformation, 122*, Article 103411. https://doi.org/10.1016/j.jag.2023.103411

Huai, Y., Lo, H. K., & Ng, K. F. (2021). Monocentric versus polycentric urban structure: Case study in Hong Kong. *Transportation Research Part A: Policy and Practice, 151*, 99–118. https://doi.org/10.1016/j.tra.2021.05.004

Hubei Meteorological Bureau. Available at: http://hb.cma.gov.cn/. [Acess in. January, 19, 2023].

Jiménez-Muñoz, J. C., & Sobrino, J. A. (2003). A generalized single-channel method for retrieving land surface temperature from remote sensing data. *Journal of Geophysical Research: Atmospheres, 108*(D22). https://doi.org/10.1029/2003JD003480, 2003JD003480.

Jones, M. C. (1993). Simple boundary correction for kernel density estimation. *Statistics and Computing, 3*(3), 135–146. https://doi.org/10.1007/BF00147776

Kedia, S., Bhakare, S. P., Dwivedi, A. K., Islam, S., & Kaginalkar, A. (2021). Estimates of change in surface meteorology and urban heat island over northwest India: Impact of urbanization. *Urban Climate, 36*. https://doi.org/10.1016/j.uclim.2021.100782

Kendall, M. G. (1973). Rank correlation methods. *International Statistical Review /Revue Internationale de Statistique, 41*(3), 399. https://doi.org/10.2307/1402637

Kim, H., Jung, Y., & Oh, J. I. (2019). Transformation of urban heat island in the three-center city of Seoul, South Korea: The role of master plans. *Land Use Policy, 86*, 328–338. https://doi.org/10.1016/j.landusepol.2019.05.016

Li, G., Zhang, X., Mirzaei, P. A., Zhang, J., & Zhao, Z. (2018). Urban heat island effect of a typical valley city in China: Responds to the global warming and rapid urbanization. *Sustainable Cities and Society, 38*, 736–745. https://doi.org/10.1016/j.scs.2018.01.033

Li, H., Zhou, Y., Jia, G., Zhao, K., & Dong, J. (2022). Quantifying the response of surface urban heat island to urbanization using the annual temperature cycle model. *Geoscience Frontiers, 13*(1). https://doi.org/10.1016/j.gsf.2021.101141

Li, K., Xia, T., & Li, W. (2021). Evaluation of subjective feelings of outdoor thermal comfort in residential areas: A case study of Wuhan. 10.3390/buildings.

Li, X., Zhou, Y., Asrar, G. R., Imhoff, M., & Li, X. (2017). The surface urban heat island response to urban expansion: A panel analysis for the conterminous United States. *Science of the Total Environment, 605-606*, 426–435. https://doi.org/10.1016/j.scitotenv.2017.06.229

Li, Z. L., & Becker, F. (1993). Feasibility of land surface temperature and emissivity determination from AVHRR data. *Remote Sensing of Environment, 43*(1), 67–85. https://doi.org/10.1016/0034-4257(93)90065-6

Liang, L., Wang, Z., & Li, J. (2019). The effect of urbanization on environmental pollution in rapidly developing urban agglomerations. *Journal of Cleaner Production, 237*. https://doi.org/10.1016/j.jclepro.2019.117649

Mann, H. B. (1945). Nonparametric tests against trend. *Econometrica : journal of the Econometric Society, 13*(3), 245. https://doi.org/10.2307/1907187

Mills, J. W. (2008). Geospatial analysis: A comprehensive guide to principles, techniques, and software tools, second edition - by Michael J. de Smith, Michael F. Goodchild, and Paul A. Longley. *Transactions in GIS, 12*(5), 645–647. https://doi.org/10.1111/j.1467-9671.2008.01122.x

Moazzam, M. F. U., Doh, Y. H., & Lee, B. G. (2022). Impact of urbanization on land surface temperature and surface urban heat Island using optical remote sensing data: A case study of Jeju Island, Republic of Korea. *Building and Environment, 222*. https://doi.org/10.1016/j.buildenv.2022.109368

Oke, T. R. (1982). The energetic basis of the urban heat island. In *Quarterly journal of the royal meteorological society, 108*.

Puplampu, D. A., & Boafo, Y. A. (2021). Exploring the impacts of urban expansion on green spaces availability and delivery of ecosystem services in the Accra metropolis. *Environmental Challenges, 5*. https://doi.org/10.1016/j.envc.2021.100283

Qian, Y., Chakraborty, T. C., Li, J., Li, D., He, C., Sarangi, C., & Leung, L. R. (2022). Urbanization impact on regional climate and extreme weather: Current understanding, uncertainties, and future research directions. *Advances in Atmospheric Sciences, 39*(6), 819–860. https://doi.org/10.1007/s00376-021-1371-9. Science Press.

Qiao, Z., Tian, G., Zhang, L., & Xu, X. (2014). Influences of urban expansion on urban heat Island in Beijing during 1989–2010. *Advances in Meteorology, 2014*, 1–11. https://doi.org/10.1155/2014/187169

Ridd, M. K. (1995). Exploring a V-I-S (vegetation-impervious surface-soil) model for urban ecosystem analysis through remote sensing: Comparative anatomy for cities†. *International Journal of Remote Sensing, 16*(12), 2165–2185. https://doi.org/10.1080/01431169508954549

Simwanda, M., & Murayama, Y. (2018). Spatiotemporal patterns of urban land use change in the rapidly growing city of Lusaka, Zambia: Implications for sustainable urban development. *Sustainable Cities and Society, 39*, 262–274. https://doi.org/10.1016/j.scs.2018.01.039

Sobrino, J. A., & Raissouni, N. (2000). Toward remote sensing methods for land cover dynamic monitoring: Application to Morocco. *International Journal of Remote Sensing, 21*(2), 353–366. https://doi.org/10.1080/014311600210876

Son, N. T., Chen, C. F., Chen, C. R., Thanh, B. X., & Vuong, T. H. (2017). Assessment of urbanization and urban heat islands in Ho Chi Minh City, Vietnam using Landsat data. *Sustainable Cities and Society, 30*, 150–161. https://doi.org/10.1016/j.scs.2017.01.009

Song, Y. (2005). Smart growth and urban development pattern: A comparative study. *International Regional Science Review, 28*(2), 239–265. https://doi.org/10.1177/0160017604273854

Sultana, S., & Satyanarayana, A. N. V. (2020). Assessment of urbanisation and urban heat Island intensities using landsat imageries during 2000 –2018 over a sub-tropical Indian City. *Sustainable Cities and Society, 52*. https://doi.org/10.1016/j.scs.2019.101846

Sussman, H. S., Raghavendra, A., & Zhou, L. (2019). Impacts of increased urbanization on surface temperature, vegetation, and aerosols over Bengaluru, India. *Remote Sensing Applications: Society and Environment, 16*. https://doi.org/10.1016/j.rsase.2019.100261

Tang, C., & Dou, J. (2022). Exploring the polycentric structure and driving mechanism of urban regions from the perspective of innovation network. *Frontiers in Physics, 10*. https://doi.org/10.3389/fphy.2022.855380

Theodorou, P. (2022). The effects of urbanisation on ecological interactions. In *Current opinion in insect science, 52*. Elsevier Inc. https://doi.org/10.1016/j.cois.2022.100922

Tran, D. X., Pla, F., Latorre-Carmona, P., Myint, S. W., Caetano, M., & Kieu, H. V. (2017). Characterizing the relationship between land use land cover change and land surface temperature. *ISPRS Journal of Photogrammetry and Remote Sensing, 124*, 119–132. https://doi.org/10.1016/j.isprsjprs.2017.01.001

Wang, W., Mao, F., Pan, Z., Du, L., & Gong, W. (2017). Validation of VIIRS AOD through a comparison with a sun photometer and MODIS AODs over Wuhan. *Remote Sensing, 9*(5), 403. https://doi.org/10.3390/rs9050403

Ward, K., Lauf, S., Kleinschmit, B., & Endlicher, W. (2016). Heat waves and urban heat islands in Europe: A review of relevant drivers. *Science of the Total Environment, 569–570*, 527–539. https://doi.org/10.1016/j.scitotenv.2016.06.119

Xie, Q., & Sun, Q. (2021). Monitoring thermal environment deterioration and its dynamic response to urban expansion in Wuhan, China. *Urban Climate, 39*. https://doi.org/10.1016/j.uclim.2021.100932

Yang, F., Lau, S. S. Y., & Qian, F. (2010). Summertime heat island intensities in three high-rise housing quarters in inner-city Shanghai China: Building layout, density and greenery. *Building and Environment, 45*(1), 115–134. https://doi.org/10.1016/j.buildenv.2009.05.010

Yang, J., Wang, Z. H., Kaloush, K. E., & Dylla, H. (2016). Effect of pavement thermal properties on mitigating urban heat islands: A multi-scale modeling case study in Phoenix. *Building and Environment, 108*, 110–121. https://doi.org/10.1016/j.buildenv.2016.08.021

Yao, J., Xu, P., & Huang, Z. (2021). Impact of urbanization on ecological efficiency in China: An empirical analysis based on provincial panel data. *Ecological Indicators, 129*. https://doi.org/10.1016/j.ecolind.2021.107827

Yin, C., Yuan, M., Lu, Y., Huang, Y., & Liu, Y. (2018). Effects of urban form on the urban heat island effect based on spatial regression model. *Science of The Total Environment, 634*, 696–704. https://doi.org/10.1016/j.scitotenv.2018.03.350

Yue, W., Liu, X., Zhou, Y., & Liu, Y. (2019a). Impacts of urban configuration on urban heat island: An empirical study in China mega-cities. *Science of the Total Environment, 671*, 1036–1046. https://doi.org/10.1016/j.scitotenv.2019.03.421

Yue, W., Qiu, S., Xu, H., Xu, L., & Zhang, L. (2019b). Polycentric urban development and urban thermal environment: A case of Hangzhou, China. *Landscape and Urban Planning, 189*, 58–70. https://doi.org/10.1016/j.landurbplan.2019.04.008

Zhang, M., Kafy, A. Al, Xiao, P., Han, S., Zou, S., Saha, M., & Tan, S (2023). Impact of urban expansion on land surface temperature and carbon emissions using machine learning algorithms in Wuhan, China. *Urban Climate, 47*, Article 101347. https://doi.org/10.1016/j.uclim.2022.101347

Zhang, Q., Wu, Z., Yu, H., Zhu, X., & Shen, Z. (2020). Variable urbanization warming effects across metropolitans of China and relevant driving factors. *Remote Sensing, 12*(9). https://doi.org/10.3390/RS12091500

Zhang, T., & Huang, X. (2018). Monitoring of urban impervious surfaces using time series of high-resolution remote sensing images in rapidly urbanized areas: A case study of Shenzhen. *IEEE Journal of Selected Topics in Applied Earth Observations and Remote Sensing, 11*(8), 2692–2708. https://doi.org/10.1109/JSTARS.2018.2804440

Zhao, M., Cai, H., Qiao, Z., & Xu, X. (2016). Influence of urban expansion on the urban heat island effect in Shanghai. *International Journal of Geographical Information Science, 30*(12), 2421–2441. https://doi.org/10.1080/13658816.2016.1178389

Zhou, D., Xiao, J., Bonafoni, S., Berger, C., Deilami, K., Zhou, Y., & Sobrino, J. A. (2019). Satellite remote sensing of surface urban heat islands: Progress, challenges, and perspectives. In *Remote sensing, 11*. MDPI AG. https://doi.org/10.3390/rs11010048

Zhou, D., Zhang, L., Hao, L., Sun, G., Liu, Y., & Zhu, C. (2016). Spatiotemporal trends of urban heat island effect along the urban development intensity gradient in China. *Science of the Total Environment, 544*, 617–626. https://doi.org/10.1016/j.scitotenv.2015.11.168

Zhou, X., & Chen, H. (2018). Impact of urbanization-related land use land cover changes and urban morphology changes on the urban heat island phenomenon. *Science of The Total Environment, 635*, 1467–1476. https://doi.org/10.1016/j.scitotenv.2018.04.091